Frontiers of Information Technology & Electronic Engineering
www.jzus.zju.edu.cn; engineering.cae.cn; www.springerlink.com
ISSN 2095-9184 (print); ISSN 2095-9230 (online)
E-mail: jzus@zju.edu.cn

Correspondence:

Frequency–angle two-dimensional reflection coefficient modeling based on terahertz channel measurement*

Zhaowei CHANG†1, Jianhua ZHANG†‡1, Pan TANG1, Lei TIAN1, Li YU1, Guangyi LIU2, Liang XIA2

[1]*State Key Laboratory of Networking and Switching Technology, Beijing University of Posts and Telecommunications, Beijing 100876, China*

[2]*China Mobile Research Institute, Beijing 100053, China*

†E-mail: changzw12345@bupt.edu.cn; jhzhang@bupt.edu.cn

Received July 5, 2022; Revision accepted Dec. 4, 2022; Crosschecked Mar. 2, 2023

https://doi.org/10.1631/FITEE.2200290

Terahertz (THz) channel propagation characteristics are vital for the design, evaluation, and optimization of THz communication systems. Moreover, reflection plays a significant role in channel propagation. In this correspondence, the reflection coefficients of the THz channel are researched based on extensive measurement campaigns. First, we set up the THz channel sounder from 220 to 320 GHz at incident angles ranging from 10° to 80°. Based on the measured propagation loss, the reflection coefficients of five building materials, i.e., glass, tile, board, plasterboard, and aluminum alloy are calculated separately for frequencies and incident angles. It is found that the lack of THz-relative parameters leads to an inability to successfully fit the Fresnel model of nonmetallic materials to the measurement data. Thus, we propose a frequency–angle two-dimensional reflection coefficient (FARC) model by modifying the Fresnel model with the Lorenz and Drude models. The proposed model characterizes the frequency and incident angle for reflection coefficients and shows low root-mean-square error (RMSE) with the measurement data. Generally, these results are useful for modeling THz channels.

1 Introduction

To meet the increasing demand for higher data rates, THz communication between 0.1 and 10 THz is attracting a great deal of attention due to its wide bandwidth, which can support much higher data rates from tens of Gb/s to a few Tb/s than millimeter wave (mmWave) communication (Zhang et al., 2017; Chen et al., 2019; Zhu et al., 2020). THz channel propagation characteristics play an important role in the design, evaluation, and optimization of THz communication systems (Eckhardt et al., 2019). Furthermore, due to the short wavelength at THz bands, the propagation mechanisms, i.e., reflection and diffraction, may change (Zhang et al., 2019, 2020). Therefore, it is quite necessary to measure and model the reflection coefficients at THz bands.

Recently, several measurement campaigns have been conducted to characterize reflection coefficients at THz bands. For example, reflection coefficients of materials were measured in Alawnch et al. (2018) with a dielectric lens antenna from 207 to 247 GHz. In Xing et al. (2019), measurements of reflection coefficients with incident angles of 10°, 30°, 60°, and 80°

‡ Corresponding author

* Project supported by the National Key R&D Program of China (No. 2020YFB1805002), the National Science Fund for Distinguished Young Scholars (No. 61925102), the National Natural Science Foundation of China (Nos. 62031019, 92167202, and 62101069), and the BUPT-CMCC Joint Innovation Center

ORCID: Zhaowei CHANG, https://orcid.org/0000-0002-8689-410X; Jianhua ZHANG, https://orcid.org/0000-0002-6492-3846

© Zhejiang University Press 2023

were carried out for drywall at 142 GHz. Piesiewicz et al. (2005) presented a measurement of reflection coefficients by THz time-domain spectroscopy (THz-TDS) for different building materials from 70 to 350 GHz at angles ranging from 20° to 75°. In Kokkoniemi et al. (2016), THz-TDS measurements were conducted from 100 GHz to 4 THz at incident angles ranging from 35° to 70°. In short, reflection coefficients of different materials have been measured in some THz bands. However, the dependence of reflection coefficients on frequencies, incident angles, and materials has been only partially investigated. Also, there is still no comprehensive model that can accurately describe the above-mentioned dependence.

The contributions of this correspondence are as follows:

1. We present an extensive reflection coefficient measurement at frequencies ranging from 220 to 320 GHz and incident angles ranging from 10° to 80°. The extensive measurement data are collected with five building materials, i.e., glass, tile, board, plasterboard, and aluminum alloy.

2. We investigate the dependence of reflection coefficients on frequencies, incident angles, and materials based on the measurement data and Fresnel model, which provides guidance for modeling reflection coefficients.

3. By modifying the Fresnel model with the Lorenz and Drude models, we propose the FARC model at THz bands. Based on the measurement results, sets of fitted parameters of different materials are obtained using the FARC model. The FARC model can successfully describe the dependence of reflection coefficients on frequencies and incident angles.

2 Measurement of terahertz reflection coefficients

The measurement of reflection coefficients is conducted by a wideband channel sounder. The details of the channel sounder can be referenced in Tang et al. (2021). The measurement setup, procedures, and data processing are introduced in this section.

2.1 Measurement setup and procedures

The measurement of reflection coefficients is conducted in a 25 °C clean room. Before installing the channel sounder, the system is calibrated after the frequency mixers are connected to each other without antennas. System calibration was introduced in Tang et al. (2021). After installing the channel sounder, the two antennas are aligned d_{ref} (d_{ref}=10 cm) apart to obtain the reference power P_{ref}. Then the five building materials (i.e., glass, tile, board, plasterboard, and aluminum alloy) are fixed at the clamp successively with the transmitter (TX) and receiver (RX) antennas being set as shown in Fig. 1a. The distances between the TX antenna and the materials (d_{t}) and between the RX antenna and the materials (d_{r}) are both 5 cm. The sketch of the measurement setup is shown in Fig. 1b. The reflection coefficients of the vertically polarized signal are measured from 10° to 80° in a step of 10°. In addition, the measurement is performed from 220 to 320 GHz in a step of 10 GHz except 270 and 310 GHz. These two frequency points are not measured because the measurement system is unstable when measuring. For each measurement, 50 snapshots of in-phase and quadrature (IQ) data are collected.

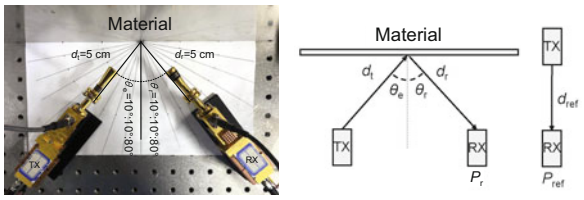

(a) (b)

Fig. 1 Terahertz reflection coefficient measurement setup: (a) actual measurement; (b) sketch

2.2 Data processing

The formula calculating the reflection coefficient can be expressed as (Landron et al., 1993)

$$|\Gamma| = \frac{d_{\mathrm{t}} + d_{\mathrm{r}}}{d_{\mathrm{ref}}} \sqrt{\frac{P_{\mathrm{r}}}{P_{\mathrm{ref}}}}, \tag{1}$$

where P_{r} is the power received by reflection. P_{r} and P_{ref} are calibrated due to systematic deviation.

3 Analysis of reflection characteristics

This section shows the reflection coefficient results of five materials. First, the dependence of reflection coefficients on frequencies and incident angles is investigated by comparing the measurement

results with theoretical modeling. Then, based on comparisons, the relationships between the reflection coefficients and five materials are described.

3.1 Frequency and angle dependence of reflection coefficients

To investigate the frequency and angle dependence of reflection coefficients, the reflection coefficients of five materials are plotted from 10° to 80° at different frequency points (Fig. 2). The results at nine frequency points are shown. For comparison, the Fresnel reflection coefficient model is plotted and the formula is given as (Landron et al., 1993)

$$\Gamma = \mathrm{e}^{-8(\frac{\pi\sigma\cos\theta_\mathrm{e}}{\lambda})^2}\left(\frac{\cos\theta_\mathrm{e}-\sqrt{\delta-\sin^2\theta_\mathrm{e}}}{\cos\theta_\mathrm{e}+\sqrt{\delta-\sin^2\theta_\mathrm{e}}}\right), \quad (2)$$

where θ_e is the incident angle, σ is the standard deviation of the surface roughness, λ is the wavelength, and δ is the relative permittivity. The relative properties of five materials in the Fresnel model are summarized in Table 1. The relative properties are theoretical values of conventional materials in the standard environment.

The angle dependence of reflection coefficients can be observed in Figs. 2a–2e. We can see that the trends of the measurement results and the Fresnel model are similar. Because of the difference between the relative parameters used in the Fresnel model and the THz measurement, there is a deviation between the results of non-metallic materials and the theoretical results. In Figs. 2a–2d, the reflection coefficients and the growth rates of non-metallic materials increase with the increase of the incident angle. Furthermore, the growth rate obviously increases when the incident angle is $\geq$50°. The same trends of reflection coefficients at different frequency bands can be found in Ahmadi-Shokouh et al. (2011) and Kim et al. (2021). The reflection coefficients of metallic materials are stable at around 0.8 in Fig. 2e, and the measurement results of the aluminum alloy are lower than the theoretical results. The reason is that the aluminum alloy may be covered with metallic oxide. The frequency dependence of reflection coefficients can also be observed in Figs. 2a–2e. The obvious fluctuations are observed by comparing reflection coefficients with frequency. Moreover, the fluctuations are related to frequency at the same incident angle. The fluctuations of plasterboard and board are within 0.2, which are smaller than those of the other three materials.

Table 1 Relative properties of five materials

Material	δ (F/m)	σ (μm)
Glass	3.5	0.006
Tile	5.5	0.050
Board	2.8	4.800
Plasterboard	1.8	2.200
Aluminum alloy	∞	4.000

δ: relative permittivity; σ: standard deviation of the surface roughness

3.2 Material dependence of reflection coefficients

To research the material dependence of reflection coefficients, the average reflection coefficients of five materials are shown in Fig. 2f in the 220–320 GHz frequency range. The average reflection coefficients are the average of the measured reflection coefficients at eight angles. Comparing the average reflection coefficients of these five materials, the average reflection coefficients of aluminum alloy are approximately 0.28 higher than that of tile and almost 0.50 higher than that of plasterboard. The aluminum alloy having the largest complex dielectric constant reflects more power, and then in turn tile, glass, board, and plasterboard. In short, the materials with larger complex dielectric constants can reflect more power.

4 Reflection coefficient modeling

In this section, an FARC model is proposed to describe the dependence of reflection coefficients on frequencies, incident angles, and materials.

The FARC model is inspired by the Lorenz, Drude, and Fresnel reflection coefficient models. The Lorenz model representing the relationship between frequency and dielectric constant of non-metallic materials is written as follows (Popescu, 2010):

$$\delta_\mathrm{L} = 1 + \frac{\omega_\mathrm{p}^2}{\omega_0^2-\omega^2-\mathrm{j}\gamma\omega}, \quad (3)$$

where

$$\omega_\mathrm{p}^2 = \frac{Ne^2}{m\epsilon_0}, \quad (4)$$

j is the imaginary unit, N is the number of electrons per unit volume, e is the unit positive charge, m is the mass of an electron, ϵ_0 is the permittivity of vacuum, γ is the damping constant, ω_0 is the resonant

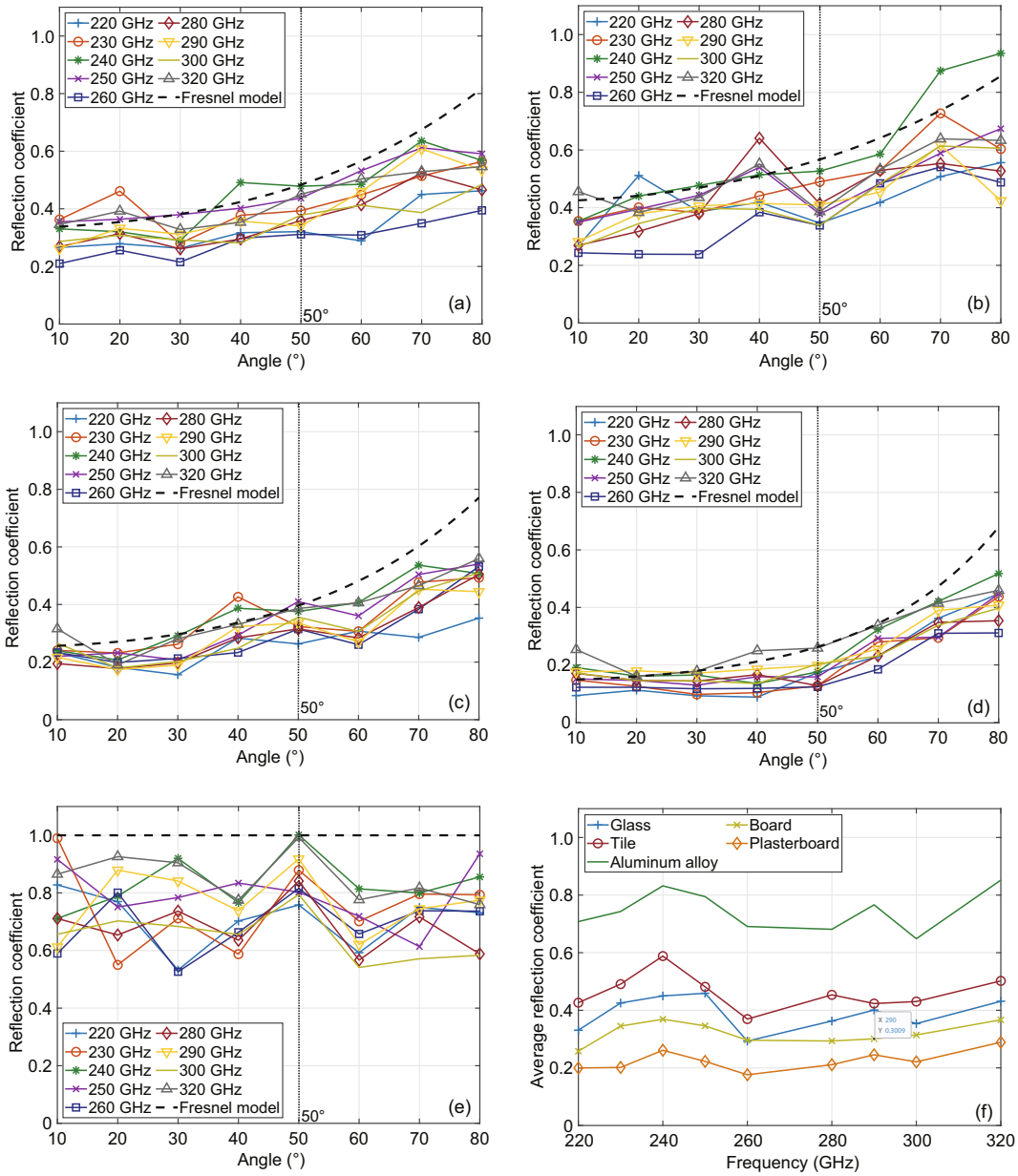

Fig. 2 Measurement results of reflection coefficients of glass (a), tile (b), board (c), plasterboard (d), and aluminum alloy (e) at nine frequency points compared with the calculation results obtained using the Fresnel model, and the average reflection coefficients of five materials at eight angles (f)

frequency, and ω is the angular velocity. Here, we choose $e = 1.6 \times 10^{-19}$ C, $m = 9.3 \times 10^{-31}$ kg, and $\epsilon_0 = 8.85 \times 10^{-12}$ F/m. The Drude model representing the relationship between frequency and dielectric constant of metallic materials is expressed as follows (Popescu, 2010):

$$\delta_{\mathrm{D}} = 1 - \frac{\omega_{\mathrm{p}}^2}{\omega^2 + \mathrm{j}\gamma\omega}. \tag{5}$$

In Eqs. (3) and (5), $\omega = 2\pi f$, where f is the frequency. Therefore, the Lorenz and Drude models can describe the dielectric constant continuously with frequency. To characterize the reflection coefficients in the Fresnel model at consecutive frequencies, the dielectric constants of non-metallic and metallic materials should be expressed by the Lorenz and Drude models, respectively. Thus, we substitute Eqs. (3) and (5) into Eq. (2). The FARC model of

the non-metallic materials is written as

$$\Gamma_{\mathrm{NM}} = \mathrm{e}^{-8(\frac{\pi\sigma\cos\theta_{\mathrm{e}}}{\lambda})^2} \cdot \left(\frac{\cos\theta_{\mathrm{e}} - \sqrt{1+\frac{\omega_{\mathrm{p}}^2}{\omega_0^2-\omega^2-\mathrm{j}\gamma\omega} - \sin^2\theta_{\mathrm{e}}}}{\cos\theta_{\mathrm{e}} + \sqrt{1+\frac{\omega_{\mathrm{p}}^2}{\omega_0^2-\omega^2-\mathrm{j}\gamma\omega} - \sin^2\theta_{\mathrm{e}}}} \right), \tag{6}$$

and the FARC model of metallic materials is expressed as

$$\Gamma_{\mathrm{MM}} = \mathrm{e}^{-8(\frac{\pi\sigma\cos\theta_{\mathrm{e}}}{\lambda})^2} \cdot \left(\frac{\cos\theta_{\mathrm{e}} - \sqrt{1-\frac{\omega_{\mathrm{p}}^2}{\omega^2+\mathrm{j}\gamma\omega} - \sin^2\theta_{\mathrm{e}}}}{\cos\theta_{\mathrm{e}} + \sqrt{1-\frac{\omega_{\mathrm{p}}^2}{\omega^2+\mathrm{j}\gamma\omega} - \sin^2\theta_{\mathrm{e}}}} \right). \tag{7}$$

The FARC model can calculate the reflection coefficients with physical parameters of materials such as σ, γ, ω_0, and ω_{p}^2. Because the Fresnel, Lorenz, and Drude models that derive the FARC model are not frequency- or material-limited, the FARC model does not have restrictions on these two dimensions. Moreover, the FARC model describes the reflection coefficients with frequency and angle in wide-frequency bands continuously with only one set of physical parameters. The Fresnel model describes the reflection coefficients at different frequencies by changing the frequency-dependent dielectric coefficients and cannot directly use frequency as a variable to describe the reflection coefficient. Thus, compared with the two-dimensional dependence described by FARC, the Fresnel model involves only the one-dimensional dependence, i.e., angle.

We change ω and λ to $2\pi f$ and c/f respectively, where f is in GHz and c is the speed of light. To characterize the model more simply, we separate θ_{e} and f in Eqs. (6) and (7). For example, Eq. (6) can be deduced as

$$\Gamma'_{\mathrm{NM}} = \mathrm{e}^{-\frac{8\pi^2\sigma^2}{c^2}f^2\cos^2\theta_{\mathrm{e}}} \cdot \left(\frac{\cos\theta_{\mathrm{e}} - \sqrt{1+\frac{\frac{\omega_{\mathrm{p}}^2}{2\pi\gamma}}{\frac{\omega_0^2}{2\pi\gamma}-\frac{2\pi}{\gamma}f^2-\mathrm{j}f} - \sin^2\theta_{\mathrm{e}}}}{\cos\theta_{\mathrm{e}} + \sqrt{1+\frac{\frac{\omega_{\mathrm{p}}^2}{2\pi\gamma}}{\frac{\omega_0^2}{2\pi\gamma}-\frac{2\pi}{\gamma}f^2-\mathrm{j}f} - \sin^2\theta_{\mathrm{e}}}} \right). \tag{8}$$

We set the separated physical parameters of the same materials in Eq. (8) to constants. Moreover, because of the large magnitudes of $8\pi^2\sigma^2/c^2$, $\omega_{\mathrm{p}}^2/(2\pi\gamma)$, and $\omega_0^2/(2\pi\gamma)$, we use powers of 10 to reduce their fitting complexity. Thus, the statistical FARC model of non-metallic materials can be written as

$$\Gamma_{\mathrm{NMS}} = \mathrm{e}^{-10^a f^2\cos^2\theta_{\mathrm{e}}} \cdot \left(\frac{\cos\theta_{\mathrm{e}} - \sqrt{1+\frac{10^b}{10^c-df^2-\mathrm{j}f} - \sin^2\theta_{\mathrm{e}}}}{\cos\theta_{\mathrm{e}} + \sqrt{1+\frac{10^b}{10^c-df^2-\mathrm{j}f} - \sin^2\theta_{\mathrm{e}}}} \right), \tag{9}$$

where a, b, c, and d can be derived as $\lg(8\pi^2\sigma^2/c^2)$, $\lg(\omega_{\mathrm{p}}^2/(2\pi\gamma))$, $\lg(\omega_0^2/(2\pi\gamma))$, and $2\pi/\gamma$, respectively. They do not have the exact physical meaning. However, these parameters are related to several physical parameters; i.e., a, b, c, and d are related to the surface roughness of the materials, the ratio of the charge per unit volume to damping constant, the ratio of the resonant frequency to damping constant, and the damping constant, respectively. Therefore, a, b, c, and d can be seen as constants to be fitted statistically. Moreover, the statistical FARC model of metallic materials can be obtained in the same way. The statistical FARC model of metallic materials is expressed as

$$\Gamma_{\mathrm{MMS}} = \mathrm{e}^{-10^a f^2\cos^2\theta_{\mathrm{e}}} \cdot \left(\frac{\cos\theta_{\mathrm{e}} - \sqrt{1-\frac{10^b}{df^2+\mathrm{j}f} - \sin^2\theta_{\mathrm{e}}}}{\cos\theta_{\mathrm{e}} + \sqrt{1-\frac{10^b}{df^2+\mathrm{j}f} - \sin^2\theta_{\mathrm{e}}}} \right). \tag{10}$$

To verify the feasibility of this model, we fit the reflection coefficients of the five materials based on the measurement results. As a representative, the results of the materials are shown in Fig. 3. Fig. 3a shows the comparison between the FARC and Fresnel models, and the measurement results of the board at 280 GHz in the angle dimension. The parameters in the Fresnel model are set according to Table 1. The trend of the FARC model is similar to that of the Fresnel model. In addition, it is found that the FARC model fits the measurement results better than the Fresnel model at the dimension of angle. Fig. 3b shows the comparison between the calculation results obtained using the FARC model and the measurement results of the plasterboard in the two dimensions of frequency and angle. The measurement data fit well with the calculation results, and most deviation values between measurement and model results are $\leq$0.05. The fitted parameters of five materials are summarized in Table 2. These four parameters of non-metallic materials are similar because the reflection coefficient trends of non-metallic

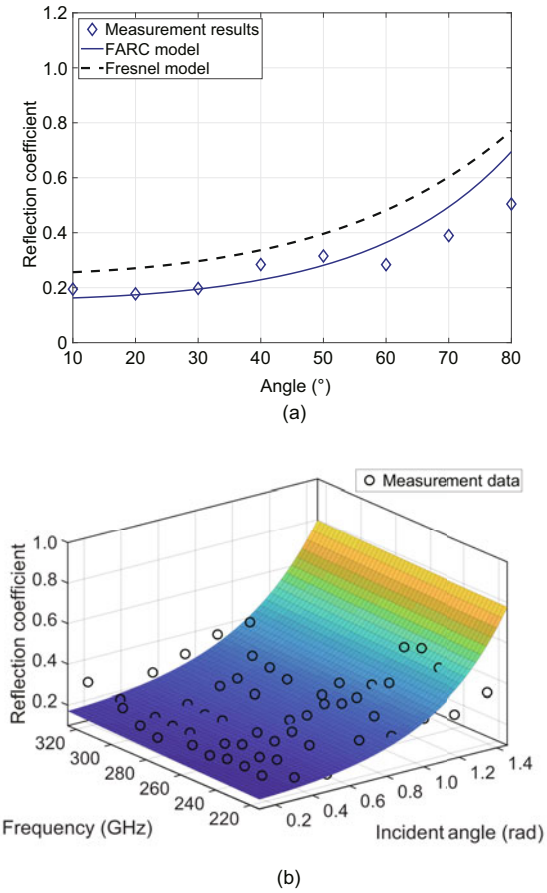

Fig. 3 Reflection coefficient fitting comparison of the board at 280 Hz in the angle dimension (a) and the plasterboard in the two dimensions of frequency and angle (b)

Table 2 Fitted parameters of five materials at nine frequency points

Material	a	b	c	d	RMSE
Glass	−15.45	3.93	3.97	0.06	0.11
Tile	−15.18	3.96	3.72	0.02	0.12
Board	−15.30	3.89	4.04	0.03	0.10
Plasterboard	−15.66	3.57	4.33	0.10	0.08
Aluminum alloy	−15.31	6.26	–	0.002	0.16

RMSE: root-mean-square error

materials varying with angle are similar. The fitted parameters of metallic materials are much different from those of non-metallic materials because their reflection coefficients have different trends. Furthermore, the RMSEs of glass, tile, board, plasterboard, and aluminum alloy are 0.11, 0.12, 0.10, 0.08, and 0.16, respectively. This demonstrates the good performance of the proposed FARC model. In summary, the proposed FARC model can characterize the frequency and angle well for reflection coefficients.

5 Conclusions

This correspondence focused on analysis and modeling in THz bands of the reflection coefficients of building materials. Based on extensive measurement campaigns from 220 to 320 GHz, we determined the reflection coefficients of five building materials. Also, the dependence of reflection coefficients on frequencies, incident angles, and materials has been investigated by comparing the measurement results with the calculation results obtained using the Fresnel model. To further describe these dependencies of reflection coefficients, an FARC model and a statistical FARC model have been proposed based on the Fresnel, Lorenz, and Drude models. By fitting all measurement data with the statistical FARC model, the reflection coefficients of five materials were obtained in continuous large bands. Generally, this work is helpful in understanding THz channel propagation mechanisms and in simulating THz channels.

Contributors

Zhaowei CHANG designed and conducted the research, processed the data, and drafted the paper. Pan TANG, Lei TIAN, Li YU, Guangyi LIU, and Liang XIA revised the paper. Jianhua ZHANG revised and finalized the paper.

Compliance with ethics guidelines

Zhaowei CHANG, Jianhua ZHANG, Pan TANG, Lei TIAN, Li YU, Guangyi LIU, and Liang XIA declare that they have no conflict of interest.

Data availability

Due to the nature of this research, participants of this study did not agree for their data to be shared publicly, so supporting data are not available.

References

Ahmadi-Shokouh J, Noghanian S, Keshavarz H, 2011. Reflection coefficient measurement for North American house flooring at 57–64 GHz. *IEEE Antenn Wirel Propag Lett*, 10:1321-1324. https://doi.org/10.1109/LAWP.2011.2177058

Alawnch I, Barowski J, Rolfes I, 2018. Extraction of relative permittivity from measured reflection coefficient of dielectric materials in the frequency range 207–247 GHz. Proc 48th European Microwave Conf, p.576-579. https://doi.org/10.23919/EuMC.2018.8541509

Chen L, Liao DG, Guo XG, et al., 2019. Terahertz time-domain spectroscopy and micro-cavity components for probing samples: a review. *Front Inform Technol Electron Eng*, 20(5):591-607. https://doi.org/10.1631/FITEE.1800633

Eckhardt JM, Doeker T, Rey S, et al., 2019. Measurements in a real data centre at 300 GHz and recent results. Proc 13th European Conf on Antennas and Propagation, p.1-5.

Kim MD, Kim KW, Kwon HK, et al., 2021. Experimental reflection characteristics of 253 GHz in a small closed-room. Proc Int Symp on Antennas and Propagation, p.689-690. https://doi.org/10.23919/ISAP47053.2021.9391212

Kokkoniemi J, Petrov V, Moltchanov D, et al., 2016. Wideband terahertz band reflection and diffuse scattering measurements for beyond 5G indoor wireless networks. Proc 22nd European Wireless Conf, p.1-6.

Landron O, Feuerstein MJ, Rappaport TS, 1993. In situ microwave reflection coefficient measurements for smooth and rough exterior wall surfaces. Proc 43rd Vehicular Technology Conf, p.77-80. https://doi.org/10.1109/VETEC.1993.510972

Piesiewicz R, Kleine-Ostmann T, Krumbholz N, et al., 2005. Terahertz characterisation of building materials. *Electron Lett*, 41(18):1002-1004. https://doi.org/10.1049/el:20052444

Popescu G, 2010. Nanobiophotonics. McGraw-Hill, New York, USA.

Tang P, Zhang JH, Tian HY, et al., 2021. Channel measurement and path loss modeling from 220 GHz to 330 GHz for 6G wireless communications. *China Commun*, 18(5):19-32. https://doi.org/10.23919/JCC.2021.05.002

Xing YC, Kanhere O, Ju SH, et al., 2019. Indoor wireless channel properties at millimeter wave and sub-terahertz frequencies. Proc IEEE Global Communications Conf, p.1-6. https://doi.org/10.1109/GLOBECOM38437.2019.9013236

Zhang JH, Tang P, Tian L, et al., 2017. 6–100 GHz research progress and challenges from a channel perspective for fifth generation (5G) and future wireless communication. *Sci China Inform Sci*, 60(8):080301. https://doi.org/10.1007/s11432-016-9144-x

Zhang JH, Kang K, Huang YM, et al., 2019. Millimeter and THz wave for 5G and beyond. *China Commun*, 16(2):iii-vi.

Zhang JH, Tang P, Yu L, et al., 2020. Channel measurements and models for 6G: current status and future outlook. *Front Inform Technol Electron Eng*, 21(1):39-61. https://doi.org/10.1631/FITEE.1900450

Zhu ZB, Hu WD, Qin T, et al., 2020. A high-precision terahertz retrodirective antenna array with navigation signal at a different frequency. *Front Inform Technol Electron Eng*, 21(3):377-383. https://doi.org/10.1631/FITEE.1900581